

Date of publication xxxx 00, 0000, date of current version xxxx 00, 0000.

Digital Object Identifier 10.1109/ACCESS.2017.Doi Number

# Magnetic Resolver Using Hall-Effect Sensors

Ye Gu Kang<sup>1</sup>, Member, IEEE, Diego F. Laborda<sup>2</sup>, Daniel Fernández<sup>2</sup>, Member, IEEE, David Reigosa<sup>2</sup>, and Fernando Briz<sup>2</sup>, Senior Member, IEEE

<sup>1</sup>Koreatech, Chungnam, South Korea

<sup>2</sup>Electrical & Electronic Dept. University of Oviedo, Gijón, Spain

Corresponding author: Ye gu Kang (e-mail: kang@koreatech.ac.kr).

This work was supported in part by the Research, Technological Development, and Innovation Programs of the Spanish Ministry of Economy and Competitiveness, under grant MINECO-17-ENE2016-80047-R, and by the Government of Asturias under project IDI/2018/000188 and FEDER funds. This paper was supported by the Education and Research promotion program of KOREATECH in 2022.

**ABSTRACT** When it comes to AC electric machines, Control requires, in many cases, accurate prediction of rotary position. Encoders and resolvers are the most general preference in the industry. Variable reluctance (VR) resolvers are a well-suited option, because of their inherent robustness in harsh environments; however, they occupy a significant portion of the total drive cost. This paper represents a magnetic resolver based on low-cost linear Hall-effect sensors, attaining desirable properties of VR resolvers. A design optimization process is proposed, and a corresponding prototype is evaluated both by finite element analysis (FEA) and experimentally. Two alternative mechanical designs are discussed: shaft and in-shaft types. Advantages of conventional encoders include compactness and a reduced cost while maintaining the advantages of VR resolvers. The proposed sensor is fully compatible with conventional drives.

**INDEX TERMS** Magnetic Resolver, Hall-sensor, angular position measurement, angular position measurement.

## I. INTRODUCTION

Electric drives are used in a large variety of applications, including domestic, industrial, traction, aerospace, etc. Precise control of AC electric machines can be achieved by accurate measurement of the rotary position. Optical encoders (optical-based angular position sensors) and resolvers (inductive-based angular position sensors) are the most used sensors in the industry [1]-[5], but many other alternatives have been reported in the literature; capacitive [2]-[3], inductive [4] or magnetic-based angular position sensors being the most extended. Capacitive-based angular position sensors in [3]-[4] provide high precision output but require additional circuitry to be compatible with standard encoder or resolver signals. Inductive position sensors are axially planar [4], low weight, with a similar operation principle to a transformer but lack robustness. Magnetic angular position sensors are mainly based on Hall-effect or Giant Magnetoresistance (GMR) devices [16]-[17], commonly used in automotive applications (e.g., throttle position detection, shaft position...) [16]-[17]. Their main drawbacks are the lack of robustness, high inertia, extra circuitry, and extra room required. In addition, their accuracy depends on offset, misalignment, or uniformity of magnetization of the permanent magnet material that must be attached to the rotating part.

In general purpose applications, Optical encoders are likely the desired option, providing incremental or absolute angular position with relatively high precision and noise immunity, but are expensive. They often exhibit a limited range of temperature of operation and a reduced capability to withstand shock and vibration, compared to resolvers.

Resolvers inherently provide the absolute position with credible precision in various circumstances: high vibration, shock, a wide range of operating temperatures, and high rotational speed. Resolvers can be brushless wound field (WF) [8], brushed (in disuse), or variable reluctance (VR) [9]-[10]. A brushless resolver is a rotary transformer, whose primary windings are stationary and secondary windings rotate, excited by AC voltage to maintain magnetic coupling with the rotor winding even at a standstill [8]. An AC voltage is induced in the output winding (stator), modulated by the rotor position. Since VR resolvers include both the output and the excitation windings in the stator without rotor windings and bearings, brushes or rotating transformer is unnecessary. VR resolvers can be frameless mounted and combined into the motor without a coupling device and additional friction to the system [7], making them attractive in traction applications (i.e., electric vehicles and hybrid electric vehicles), [7]-[8]. The drive cost, however, is the limitation [6], [11]. A special type of VR resolvers recently

proposed includes permanent magnets (PM) in the stator, i.e., field modulation PM resolvers [19]-[20]. In [19], ferrite magnets are inserted in the back iron (stator part) of the resolver to avoid the use of excitation signals at high speeds. In [20] ferrite magnets are placed in the stator teeth and due to the variable reluctance property of the rotor, variable flux leakage (sinusoidal) is produced and can be measured using Hall-effect sensors.

This paper proposes an alternative design of a magnetic resolver using field sensors (i.e., Hall-effect) and a magnetized moving part that can be made of non-laminated electrical steel and permanent magnets [24]. Compared to the VR resolver, the proposed design is simpler, more compact, cheaper, and easier manufacturability: it does not require stator/rotor laminations nor windings, the stator is made of a simple ferromagnetic ring, and the rotor is made of an optimized shape, similar to VR designs but including magnets. Despite it requires the addition of sensors and conditioning electronics, its power consumption is very low, and it can provide more than one independent output for the redundant mode of operation. **The size or the number of poles is easily scalable** to meet the requirements of a specific application. Since it maintains the main properties of the VR resolver, fully compatible with standard resolver signals, modification in the cabling or electronics of the drive is not required. This paper also describes the optimization process of the resolver geometry, a FEA analysis of the system, and the experimental validation.

The paper is organized as follows: principles of operation are discussed in Section II, design optimization is discussed in section III, and the validation of the model using FEA is presented in Section IV. Section V shows an assembly of the proposed prototype. Experimental results and conclusions are presented in sections VI and VII, respectively.

## II. PRINCIPLE OF OPERATION

A brief description of conventional resolvers aimed to establish the basis for the assessment of the proposed concept is presented following.

Resolvers can be broadly classified into brushless wound field (WF) and variable reluctance (VR). Rotor winding of WF resolvers is excited by an AC voltage, which can be produced by means of a magnetic coupling (i.e., brushless WF, see Fig. 1a). Voltages in the stator windings are *sine* and *cosine* signals, which are modulated by the rotor angle  $\theta_r$ . In VR resolvers, excitation winding is also placed in the stator (see Fig. 1b), avoiding the use of brushes or slip rings. In addition, they can be in-shaft installed. An AC voltage/current signal is injected into the excitation winding, the resulting voltages in the two stator windings being *sine* and *cosine* signals whose angle is modulated by the rotor angle as for the WF case. VR resolvers are made simple and robust, which allow a wider temperature range of operation, less sensitive to noise, and longer transmission cables [7][8].

Both are a special type of rotary transformer that couples a primary winding (*Excitation* see Fig. 1) with two secondary

windings (*Output 1 & 2*) that are 90 electrical degrees phase shifted. Excitation signal, i.e.,  $v_E(t)$  in Fig. 1, is generally a sine wave (1) (see Fig. 2a), of magnitude and angular frequency  $E_0$  and  $\omega_s$ , respectively. The output signals of the resolver are  $v_S(t)$  (2) and  $v_C(t)$  (3) (see Figs. 2b and 2c), where  $k$  is the equivalent turns ratio of the magnetic coupling,  $\theta_r$  is the rotor position and  $X$  is a multiplication factor for the angle [6].

$$v_E(t) = E_0 \sin(\omega_s t) \quad (1)$$

$$v_S(t) = E_0 \sin(\omega_s t) k \sin(X\theta_r) \quad (2)$$

$$v_C(t) = E_0 \sin(\omega_s t) k \cos(X\theta_r) \quad (3)$$

$$v'_S(t) = k \sin(X\theta_r) \quad (4)$$

$$v'_C(t) = k \cos(X\theta_r) \quad (5)$$

$v_S(t)$  and  $v_C(t)$  are the input to a resolver-to-digital (R/D) converter, which typically includes a demodulation stage to subtract the excitation signal; (4) and (5) being obtained after the demodulation. A large variety of methods have been reported to obtain the rotor position,  $\theta_r$ , from (4) and (5) [15], [21]-[23].

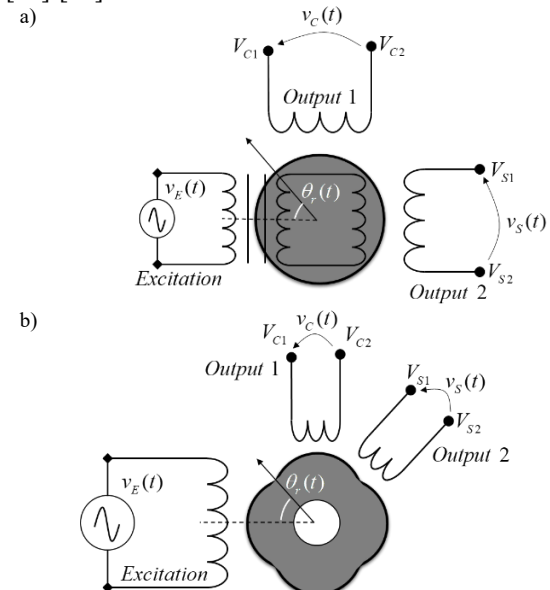
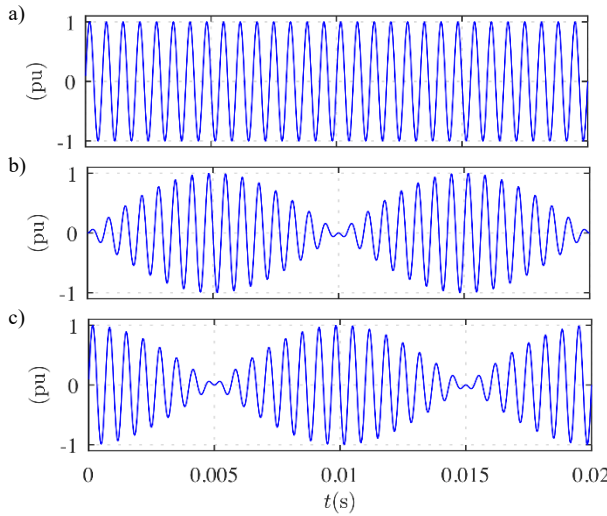


FIGURE 1. Resolvers, a) WF and b) VR.

### A. Principle of Operation of the proposed magnetic resolver

The proposed magnetic resolver is schematically shown in Fig. 3. It consists of a rotor and a stator: the rotor is made of a non-laminated ferromagnetic core and permanent magnets (PMs in Fig. 3); the stator consists of two Hall-effect sensors 90 electrical degrees phase shifted. Linear Hall-effect integrated circuit (IC) sensors will be used for the proposed magnetic resolver. These types of ICs allow current control through the Hall element without integrated electronics.



**FIGURE 2.** Resolver signals, a) excitation,  $v_e(t)$ , b) Output 1 of the resolver,  $v_c(t)$  (i.e., cosine), c) Output 2 of the resolver,  $v_s(t)$  (i.e., sine).  $\omega_s = 2 \cdot \pi \cdot 500$  rad/s,  $\omega_r = 2 \cdot \pi \cdot 50$  rad/s

Hall-effect sensors are usually fed using DC voltage (6) or current, see Fig. 4a, the output voltage (Hall voltage) of the Hall-effect sensors  $v_{HS}(t)$  and  $v_{HC}(t)$  (see Fig. 3) for the case of constant rotor speed are (7)-(8), see Fig. 4b and Fig. 4c. While these signals are modulated by the rotor position, they differ from the signals provided by conventional resolvers, where the position information signals produce an amplitude modulated carrier signal (see Fig. 2). Alternatively, the Hall-effect sensors can be fed with AC voltage (or current). The input excitation signal is (10), and the corresponding output voltages for the case of constant rotor speed will be (11)-(12), see Fig. 4d and Fig. 4f, which are equal to the signals provided by conventional resolvers. Note that or every pair of poles (p) in the rotor, four Hall-effect sensors can be installed in the rotor, providing duplicated signals for applications where redundancy is required.

It must be remarked that (11)-(12) results from a sinusoidal flux distribution in the rotor surface. Rotor design to achieve this target is described following.

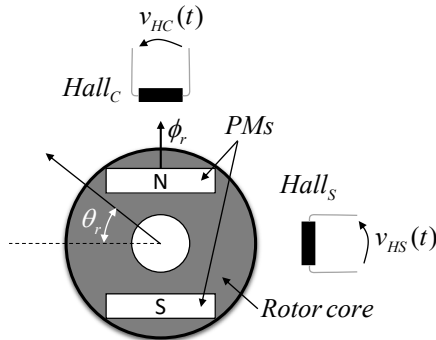


**FIGURE 3.** Schematic representation of the proposed magnetic resolver and position of the Hall-effect sensors.

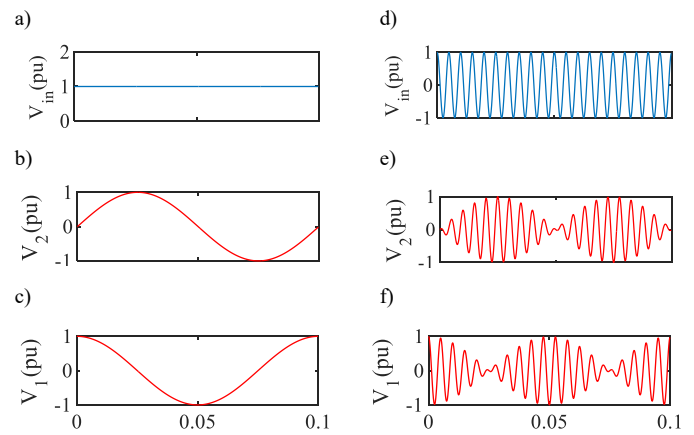


**FIGURE 4.** Excitation and resulting waveforms of the proposed resolver: a) DC excitation, b) Sin output for DC excitation, c) Cos output for DC excitation, d) AC excitation, e) Sin output for AC excitation, f) Cos output for AC excitation.

$$v_E(t) = E_0 \quad (6)$$

$$v_{HS}(t) = k \sin(\theta_r) \quad (7)$$

$$v_{HC}(t) = k \cos(\theta_r) \quad (8)$$

$$v_{Hall}(t) = k i(t) B(t) \quad (9)$$

$$v_E(t) = E_0 \sin(\omega_s t) \quad (10)$$

$$v_{HS}(t) = E_0 \sin(\omega_s t) k \sin(\theta_r) \quad (11)$$

$$v_{HC}(t) = E_0 \sin(\omega_s t) k \cos(\theta_r) \quad (12)$$

$$MO = \text{Penalty} + \sum_{n=1}^3 O_n w_n \quad (13)$$

### III. Rotor Design Optimization of the Proposed Magnetic Resolver

The optimization technique applied to the proposed magnetic resolver is explained in this section. The rotor geometry has been optimized to achieve three main targets: minimize the use of magnetic materials, maximize the fundamental flux amplitude, and minimize the harmonic distortion on the flux density waveform. Differential evolution optimization technique [13] was used to find the optimum solution in the design space using 2D finite element analysis (FEA). Rotor parameters are shown in Fig. 5 and Table. II.

The desired properties of the Hall-effect sensor-based resolver are included in the objective function variable,  $O_n$ , of the multi-objective (MO) function (13): the total harmonic distortion (THD) of the flux density,  $O_1$ , the volume of the permanent magnet (PM),  $O_2$ , and the magnitude of the airgap flux density,  $O_3$ , where  $w_n$  is the weighting factor of each objective variable. The fundamental component of the airgap flux density will determine the sensitivity of the proposed resolver, where the THD indicates the quality of the signal for the rotor position estimation. The PM volume is included

in the objective function to minimize the system cost. The goal of the multi-objective optimization is to find a minimum cost of MO (13). More details about the variable used in the multi-objective optimization are in Table I; the penalty is used for eliminating designs that violate the geometric constraints shown in Table II.

TABLE I  
PARAMETERS OF THE MULTY-OBJECTIVE FUNCTION

Symbol	Function	Definition
$O_1$	THD	Harmonic distortion of flux in %
$O_2$	$(0.08 - B_{hall})^2$	Fundamental flux amplitude in Tesla with a target amplitude of 0.08
$O_3$	PM Volume	Magnet volume in mm <sup>3</sup>
$w_1$	20	Weighting factor of $O_1$
$w_2$	20000	Weighting factor of $O_2$
$w_3$	10	Weighting factor of $O_3$
Penalty	0 if within the boundary 100 if outside boundary	Penalty is given when the input variables are outside the minimum and maximum range.

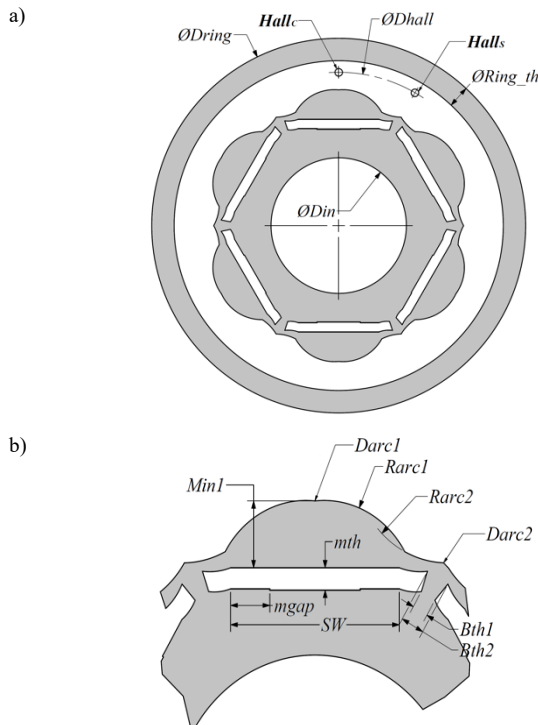


FIGURE 5. Dimensions of the magnetic resolver a), general view and b), detailed view.

The resulting optimized resolver design will be, therefore, highly sensitive to rotor position, with low harmonic distortion, and low-cost given the pre-defined boundary conditions. Three different types of permanent magnet materials have been evaluated: Sintered NdFeB, bonded NdFeB, and Ferrite magnets.

TABLE II  
GEOMETRIC PARAMETERS DESCRIPTION

Symbol	Definition
$Darc1$	Rotor d-axis outer diameter
$Darc2$	Rotor q-axis outer diameter
$\phi Dhall$	Hall sensor distance from the center
$\phi D_{in}$	Rotor inner diameter
$\phi D_{ring}$	Ring outer diameter
$Ring\_th$	Ring thickness
$Rarc1$	Rotor d-axis outer arc
$Rarc2$	Rotor q-axis outer arc
$mth$	Magnet thickness
$Min1$	Magnet distance from $\phi Darc1$
$mgap$	Magnet gap in slot
$SW$	Slot width
$Bth1$	Outer bridge thickness
$Bth2$	Inner bridge thickness

Fig. 6 shows an example of the flux distribution when using the selected geometry for the three permanent magnet materials, main properties of each case being shown in Table III. As expected, the maximum peak flux density in the airgap is obtained with the prototype equipped with sintered NdFeB magnets, see Table III. This will allow better use of the measuring range of the Hall-effect sensor, eventually improving the signal-to-noise ratio. Obtaining a similar peak flux density, bonded NdFeB magnets requires almost twice of magnetic material, see Table III. Ferrite magnets provide, as expected, the smallest flux density, with a peak value around half of that obtained with NdFeB magnets. The Ferrite vs. NdFeB volume to achieve the same peak flux density is around 2.5, see Table III. Even in this case, the ferrite-based solution is expected to be cheaper. Considering the material cost and the manufacturing cost, Ferrite based resolver is cheaper than NdFeB based resolver in mass production.

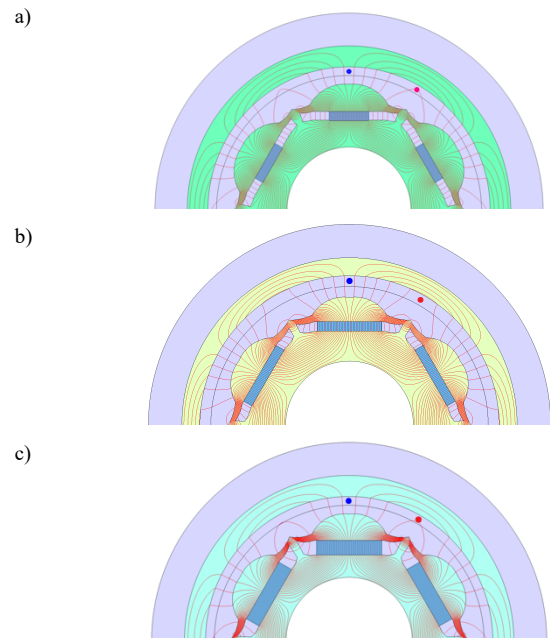


**FIGURE 6.** Flux lines distribution for the optimized magnetic resolver design equipping a) Sintered NdFeB magnets, b) Bonded NdFeB magnets, and c) Ferrite magnets. Blue (•) and red (•) spots represent the Hall<sub>C</sub> and Halls sensors.

TABLE III

OPTIMIZATION RESULTS OF THE MAGNETIC RESOLVER

	PM Material		
	Sintered NdFeB	Bonded NdFeB	Ferrite
THD (%)	0.92	1.08	1.28
Fundamental flux density amplitude (mT)	77.27	72.39	56.03
PM volume (mm <sup>3</sup> )	37.16	64.75	103.70

\*Results obtained from FEA simulation.

#### IV. Validation Of The Resolver Using FEA

This section shows FEA results for the three optimized prototypes using sintered NdFeB, bonded NdFeB, and Ferrite, respectively.

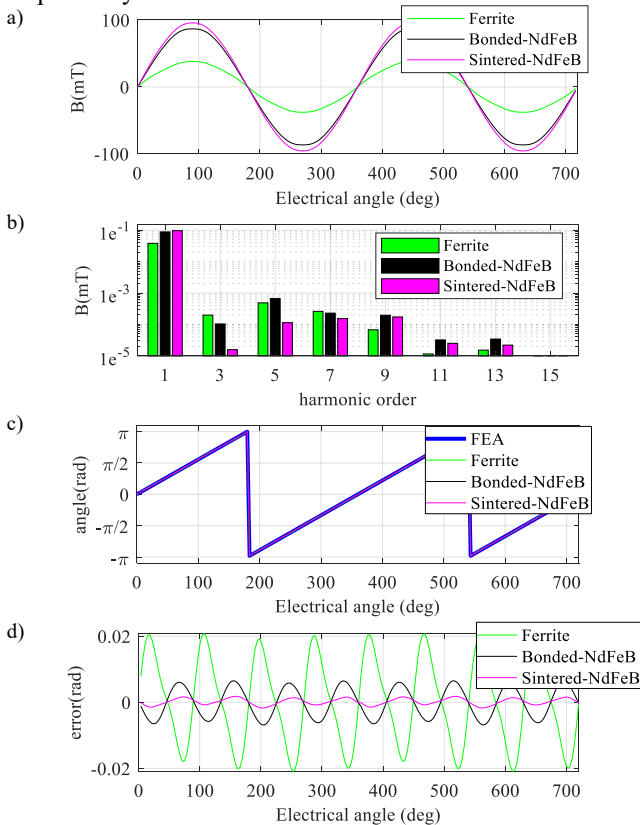


**FIGURE 7.** Performance of the three types of resolvers. a) sin output of the hall effect sensors, b) FFT of sin output (in a)), c) resulting position angle, and d) resulting angle error.

Fig. 7a shows the magnetic flux density at the position of “Hall” sensor (see Fig. 3 and 6) for one rotor revolution and for the three magnetic materials. Fig. 7b shows the corresponding FFTs, from which the THDs in Table III are obtained. It can be observed that the THD in all cases is <1.55%, all harmonics being at least two orders of magnitude smaller than the fundamental component. It is noted that these results might be influenced by the bandwidth of the Hall-Effect sensors, which is typically >250kHz [12]; i.e.,

the bandwidth of the Hall-effect sensors will have virtually no influence in standard machines used in traction applications [14]. Fig. 7c shows the measured position for the three different magnetic materials and the real position. Fig. 7d shows the error in the estimated position; variations in the errors being due to the harmonics in the flux waveform shown in Fig. 7b, i.e. they are not the results of assembling tolerances, circuitry, noise, misalignments, etc.

It can be observed in Fig. 7d that the lower error is obtained for the sintered NdFeB magnet, ferrite magnets showing the worst behavior. Measurement errors are  $\pm 1.1^\circ$  (Ferrite based),  $\pm 0.35^\circ$  (bonded NdFeB based), and  $\pm 0.09^\circ$  (sintered NdFeB based). Position error of commercially available resolvers is in the range of  $\pm 0.5\text{--}1.0^\circ$  for VR resolvers [11] and around  $\pm 0.16^\circ$  for brushless resolvers, meaning that the accuracy of the proposed system is comparable with commercially available resolvers.

#### V. Assembly Of The Proposed Prototype

The proposed prototype can be assembled in two different configurations: in-shaft mounting and shaft-type for connections through flexible couplings. In any case, the necessary circuitry is the same, both allowing redundant configuration (i.e., providing duplicated signals). Fig. 8a shows the laser cutout (silicon steel 50H350) of the optimized designs for the prototypes equipping sintered NdFeB magnets and Ferrite magnets, the PM samples being shown in Fig. 8b. The same laser cutout and magnets will be used for both the in-shaft and shaft-type resolvers.

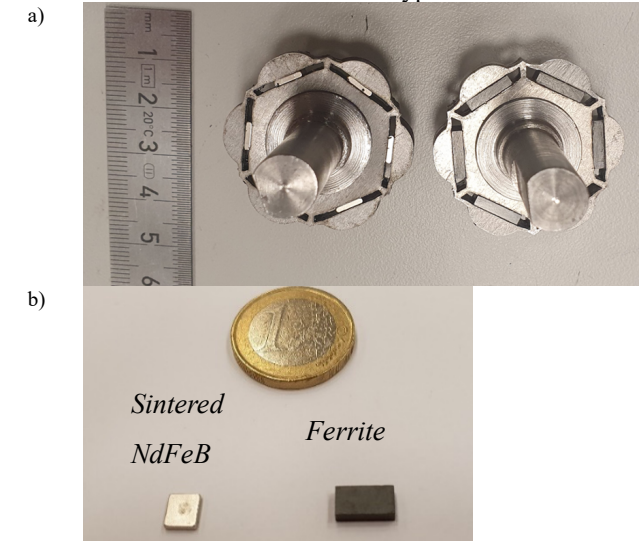


**FIGURE 8.** a) Lamination of the optimized geometries for the magnetic resolver design equipping: sintered NdFeB (left) and Ferrite (right), and b) NdFeB and Ferrite magnets for the designs in Fig. 8a.

##### A. Shaft-type assembly

The shaft-type magnetic resolver is shown in Fig. 9. It is equipped with the rotor cutout and PMs shown in Fig 8. It was designed with 8 mm shaft diameter, the diameter of the body and axial dimensions being 52 mm and 17 mm respectively. This design is suitable for the connection through flexible couplings. It can be observed that the PCB integrates four Hall-effect sensors (i.e., two Hall<sub>C</sub> and two

Halls), i.e., it provides redundant output signals. The design also includes two bearings: front and rear cover hosts.

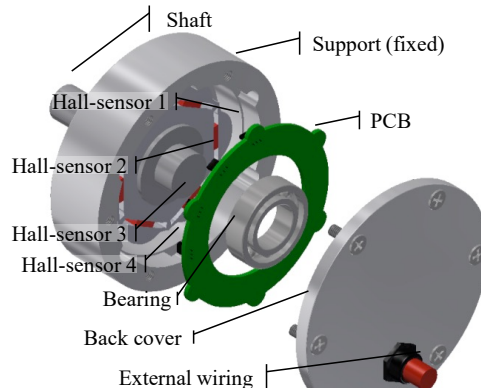


FIGURE 9. Disassemble view of the Shaft-type magnetic resolver

### B. In-shaft mount assembly

The in-shaft type magnetic resolver is shown in Fig. 10. It is equipped with the rotor cutout and PMs shown in Fig 8. The rotor of the sensor is directly connected to the machine shaft and fixed by a nut. The axial length of the sensor exploding bolts is 5 mm, and the diameter of the sensor is 70 mm. In this case, the PCB integrates only two Hall-effect sensors (i.e.,  $Hall_c$  and  $Hall_s$ ), although this design also allows redundant configuration. The advantage of this design is that it does not require bearings.

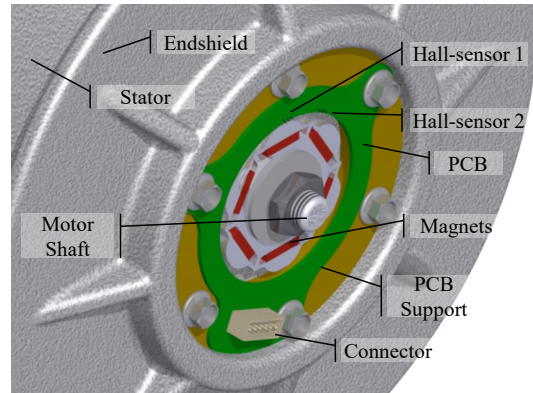


FIGURE 10. In-shaft type magnetic resolver inserted in an end-shield of a machine.

### C. Electronic circuitry

A conditioning system is required for the proposed prototype to achieve full compatibility with commercial drives in terms of power supply and output voltage levels. Its objective is twofold: provide supply voltages for the Hall elements and the additional ICs, and adapt output voltage levels within the range of commercial drives.

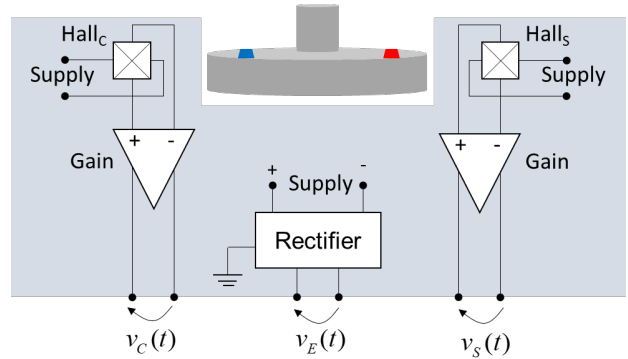


FIGURE 11. Simplified representation of the electronic circuitry.

Fig. 11 shows a simplified representation of the electronic circuit needed for the proposed sensor. The excitation signal, which will be provided by the drive (i.e., standard resolver excitation), is rectified to provide symmetrical voltage supply to the conditioning circuit, as demanded by operational amplifiers. Hall elements (i.e.,  $Hall_c$  and  $Hall_s$ ) are fed using AC voltage what produces a AC current through the hall elements since hall elements are resistors from an electrical point of view. Note that a temperature variation of the hall element will have a direct impact on the current through the hall element. However, this will not affect the position measurement since the rotor position information is embedded in the phase of the current waveforms but not in the amplitude (see Fig. 2).

The total power consumption of the proposed system is in the range of the power consumption of the Hall-elements: 12.5 mW per sensor. The power losses due to the rectification stage could be considered as negligible (i.e., conduction losses of a rectifier diode). The power consumption of the gain stages could be also considered as negligible since ultra-low-power differential operational amplifiers are used.

The circuit in Fig. 11 provides differential output signals to enhance noise immunity in the transmission wire.

## VI. Experimental Results

The prototype of the proposed system is shown in Fig. 12 corresponding to the drawing in Fig. 9. The fixed parts of the sensor (i.e., shaft, stator, data acquisition circuitry board, and cover) are shown in Fig. 12a. The assembled system with moving parts (i.e., magnets and rotor shown in Fig. 8) is shown in Fig. 12b. The sensor is attached to a brushless PMSM in a testbench. The prototype integrates two pairs of Hall-effect sensors (i.e.,  $Hall_c$  and  $Hall_s$ ) for a redundant output, the simplified power and conditioning stages for each pair of sensors being shown in Fig. 11. The prototype has been designed with large tolerances to reduce complexity and ease assembling process.

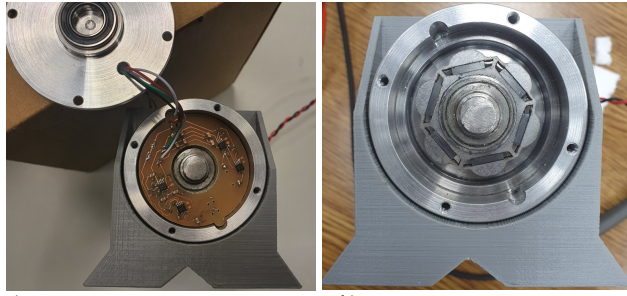


**FIGURE 12.** a) Shaft, stator and data acquisition circuitry board, b) Assembled proposed resolver.

Fig. 13 shows the output waveforms provided by a pair of Hall-effect sensors (i.e., *Hall<sub>C</sub>* and *Hall<sub>S</sub>*) when they are fed with a sinusoidal waveform of 7VRMS at 10 kHz. Fig. 13 shows the simplified signal processing used for speed and position estimation. Measured flux densities by *Hall<sub>C</sub>* and *Hall<sub>S</sub>* are multiplied by the excitation signal,  $V_a$  and  $V_b$  being obtained.  $V_a$  and  $V_b$  normalized, (14), and  $\vec{V}_{dq}^r$  (15)-(16), is obtained using a synchronous reference frame phase-locked loop (SRF-PLL), which provides the estimated rotor speed and position [18].

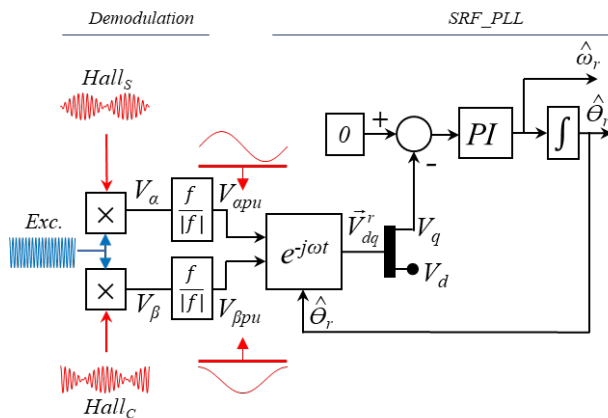


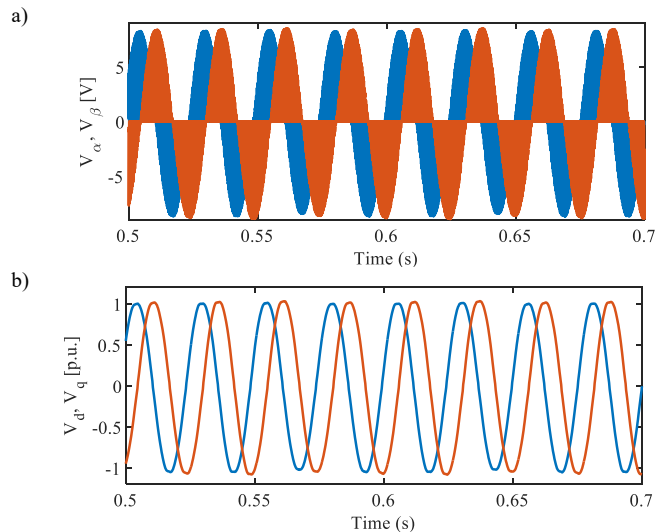
**FIGURE 13.** Schematic representation of the signal processing used for speed and position estimation.

$$V_{\alpha pu} = \frac{V_\alpha}{|V_\alpha|}; \quad V_{\beta pu} = \frac{V_\beta}{|V_\beta|} \quad (14)$$

$$\vec{V}_{\alpha\beta pu}^s = V_{\alpha pu} + jV_{\beta pu} \quad (15)$$

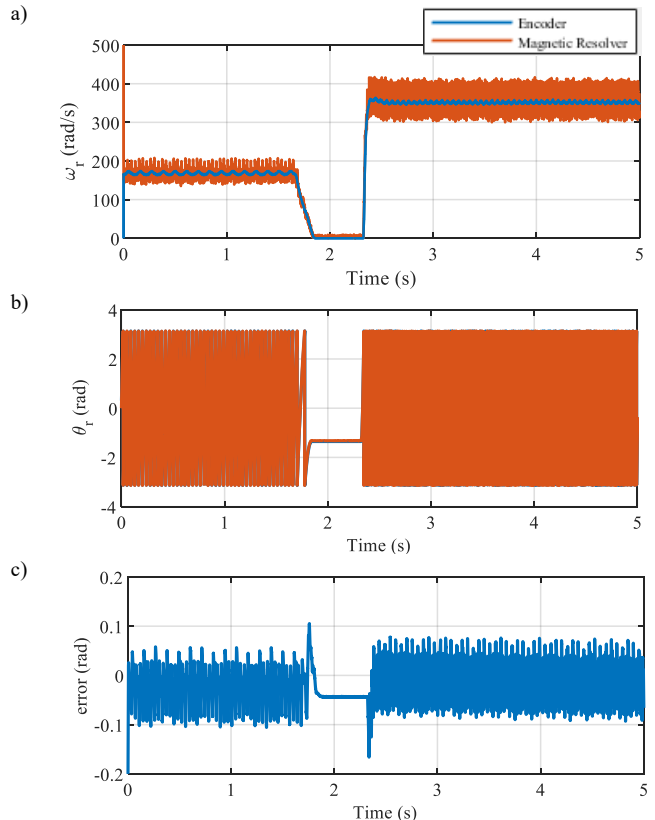
$$\vec{V}_{dq}^r = \vec{V}_{\alpha\beta pu}^s e^{-j\theta_r} \quad (16)$$

Fig. 14 shows the experimental results of the assembled resolver using the signal processing scheme in Fig. 13 with the rotor speed of 250 rad/s. The  $V_\alpha$  and  $V_\beta$  in demodulation process are shown in Fig. 14a. The output signals from SRF-PLL,  $V_d$  and  $V_q$ , are shown in Fig. 14b.



**FIGURE 14.** Magnetic resolver signals,  $\omega_s = 2 \cdot \pi \cdot 10000$  rad/s,  $\omega_r = 250$  rad/s.  
a)  $V_\alpha$ (red),  $V_\beta$ (blue), b)  $V_d$  (red),  $V_q$  (blue).

Fig. 15 shows the estimated speed and corresponding rotor position obtained from the proposed sensor during dynamic changes of the rotor velocity. The machine is rotating at 166 rad/s until 1.7 s, and decelerated to 0 rad/s until 2.3 s then accelerated to 350 rad/s. Fig. 15b and 15c show the corresponding rotor position and the position error. The maximum position error during transients being 0.165 rad.



**FIGURE 15.** Experimental results obtained with the proposed sensor,  $\omega_s = 2 \cdot \pi \cdot 10000$  rad/s. a) Speed, b) Angular position, c) Angular position error.

## VII. Conclusions

A magnetic resolver using Hall-effect sensors is proposed in this paper. Compared to available resolvers, it provides similar accuracy, with a simpler and cheaper construction. Two different designs have been proposed: shaft-type and in-shaft designs; both allowing redundant position measurement. The optimization process of the rotor geometry is shown, and FEA and experimental results have been provided to demonstrate the viability of the proposed system.

## ACKNOWLEDGMENT

Author would like to thank Bomatec AG for advising and providing magnet samples.

## REFERENCES

- [1] R. M. Kennel, "Why Do Incremental Encoders Do a Reasonably Good Job in Electrical Drives with Digital Control?," Conference Record of the 2006 IEEE Industry Applications Conference Forty-First IAS Annual Meeting, Tampa, FL, 2006, pp. 925-930. doi: 10.1109/IAS.2006.256635
- [2] B. Hou, C. Li, Z. Gao, Q. Wei, B. Zhou and R. Zhang, "Design, Optimization, and Compensation of a High-Precision Single-Excitation Absolute Capacitance Angular Encoder up to  $\pm 4''$ ," in IEEE Transactions on Industrial Electronics, vol. 66, no. 10, pp. 8161-8171, Oct. 2019. doi: 10.1109/TIE.2018.2886762
- [3] H. Pu, H. Wang, X. Liu, Z. Yu and K. Peng, "A High-Precision Absolute Angular Position Sensor With Vernier Capacitive Arrays Based on Time Grating," in IEEE Sensors Journal, vol. 19, no. 19, pp. 8626-8634, 1 Oct. 2019. doi: 10.1109/JSEN.2019.2921479
- [4] M. Howard, Incremental encoders, absolute encoders & pseudo-absolute encoders, Feb. 2013. Accessed on: Dec. 15, 2019. [Online]. Available: [https://www.zettlex.com/wp-content/uploads/2017/08/incremental-encoders-vs.-absolute-encoders\\_Rev\\_3.1.pdf](https://www.zettlex.com/wp-content/uploads/2017/08/incremental-encoders-vs.-absolute-encoders_Rev_3.1.pdf)
- [5] F. Jiang, D. Lou, H. Zhang, L. Tang, S. Sun and K. Yang, "Design of a GMR-based magnetic encoder using TLE5012B," 2017 20th International Conference on Electrical Machines and Systems (ICEMS), Sydney, NSW, 2017, pp. 1-4. doi: 10.1109/ICEMS.2017.8056197
- [6] C. Jin, I. Jang, J. Bae, J. Lee and W. Kim, "Proposal of Improved Winding Method for VR Resolver," in IEEE Transactions on Magnetics, vol. 51, no. 3, pp. 1-4, March 2015, Art no. 8102404. doi: 10.1109/TMAG.2014.2348321
- [7] L. Sun, "Analysis and Improvement on the Structure of Variable Reluctance Resolvers," in IEEE Transactions on Magnetics, vol. 44, no. 8, pp. 2002-2008, Aug. 2008. doi: 10.1109/TMAG.2008.923315
- [8] J. Figueiredo, "Resolver models for manufacturing," IEEE Trans. Ind. Electron., 58(8): 3693-3700, Aug. 2011.
- [9] L. Z. Sun, J. B. Zou, and Y. P. Lu, "New variable-reluctance resolver for rotor-position sensing," in Proc. IEEE Region 10th Conf. TENCON, vol. 4, Chiang Mai, Thailand, pp. 5-8, Nov. 2004.
- [10] H. Saneie, Z. Nasiri-Gheidari and F. Tootoonchian, "Design-Oriented Modelling of Axial-Flux Variable-Reluctance Resolver Based on Magnetic Equivalent Circuits and Schwarz-Christoffel Mapping," in IEEE Transactions on Industrial Electronics, vol. 65, no. 5, pp. 4322-4330, May 2018, doi: 10.1109/TIE.2017.2760862.
- [11] T. Suzuki, K. Toyotake and Y. Yamashita, "Variable reluctance type resolver rotor and brushless motor," Japan Patent JP2010048775A, Aug. 25, 2008.
- [12] D. Fernandez et al., "Permanent Magnet Temperature Estimation in PM Synchronous Motors Using Low-Cost Hall Effect Sensors," in IEEE Transactions on Industry Applications, vol. 53, no. 5, pp. 4515-4525, Sept.-Oct. 2017. doi: 10.1109/TIA.2017.2705580
- [13] S. Das and P. N. Suganthan, "Differential Evolution: A Survey of the State-of-the-Art," in IEEE Transactions on Evolutionary Computation, vol. 15, no. 1, pp. 4-31, Feb. 2011. doi: 10.1109/TEVC.2010.2059031
- [14] M. Minowa, H. Hijikata, K. Akatsu and T. Kato, "Variable leakage flux interior permanent magnet synchronous machine for improving efficiency on duty cycle," 2014 International Power Electronics Conference (IPEC-Hiroshima 2014 - ECCE ASIA), Hiroshima, 2014, pp. 3828-3833. doi: 10.1109/IPEC.2014.6870049
- [15] L. Pecl, R. Schindeler, D. Cleveland and K. Hashtroodi-Zaad, "High-Precision Resolver-to-Velocity Converter," in IEEE Transactions on Instrumentation and Measurement, vol. 66, no. 11, pp. 2917-2928, Nov. 2017. doi: 10.1109/TIM.2017.2714378
- [16] P. Kejik, S. Reymond and R. S. Popovic, "Circular Hall Transducer for Angular Position Sensing," TRANSDUCERS 2007 - 2007 International Solid-State Sensors, Actuators and Microsystems Conference, Lyon, 2007, pp. 2593-2596. doi: 10.1109/SENSOR.2007.4300702
- [17] K. Bienczyk, "Angle measurement using a miniature hall effect position sensor," 2009 2nd International Students Conference on Electromagnetic and Mechatronics, Silesia, 2009, pp. 21-22. doi: 10.1109/ISCON.2009.5156096
- [18] D. Reigosa, D. Fernandez, C. González, S. B. Lee and F. Briz, "Permanent Magnet Synchronous Machine Drive Control Using Analog Hall-Effect Sensors," in IEEE Transactions on Industry Applications, vol. 54, no. 3, pp. 2358-2369, May-June 2018, doi: 10.1109/TIA.2018.2802950.
- [19] L. Sun, Z. Luo, K. Wang, R. Cao and S. Ding, "A Stator-PM Resolver With Field Modulation Principle," in IEEE Transactions on Energy Conversion, vol. 36, no. 1, pp. 159-172, March 2021, doi: 10.1109/TEC.2020.3001655.
- [20] M. Bahari, A. Davoodi, H. Saneie, F. Tootoonchian and Z. Nasiri-Gheidari, "A New Variable Reluctance PM-Resolver," in IEEE Sensors Journal, vol. 20, no. 1, pp. 135-142, 1 Jan. 2020, doi: 10.1109/JSEN.2019.2941554.
- [21] S. Golestan, J. M. Guerrero and J. C. Vasquez, "Single-Phase PLLs: A Review of Recent Advances," in IEEE Transactions on Power Electronics, vol. 32, no. 12, pp. 9013-9030, Dec. 2017, doi: 10.1109/TPEL.2017.2653861.
- [22] S. Golestan, M. Monfared, F. D. Freijedo and J. M. Guerrero, "Dynamics Assessment of Advanced Single-Phase PLL Structures," in IEEE Transactions on Industrial Electronics, vol. 60, no. 6, pp. 2167-2177, June 2013, doi: 10.1109/TIE.2012.2193863.
- [23] S. Shinnaka, "A Robust Single-Phase PLL System With Stable and Fast Tracking," in IEEE Transactions on Industry Applications, vol. 44, no. 2, pp. 624-633, March-April 2008, doi: 10.1109/TIA.2008.916750.
- [24] Y. G. Kang, D. F. Laborda, D. Fernández, D. Reigosa and F. Briz, "Magnetic Resolver Using Hall-Effect Sensors," 2020 IEEE Energy Conversion Congress and Exposition (ECCE), 2020, pp. 2344-2350, doi: 10.1109/ECCE44975.2020.9236184.



**Ye gu Kang** received the B.S. degree in electrical engineering from Penn State University, State College, PA, USA, in 2011. He received the M.S. degree in electrical engineering and the Ph.D. degree in mechanical engineering from the University of Wisconsin, Madison, WI, USA, in 2013 and 2019, respectively. From 2019 to 2020, he worked as an Investigator at the University of Oviedo, Gijón, Spain. He is currently an assistant professor at KOREATECH. His research interests include the design and control of energy conversion devices.



**David Reigosa** was born in Spain 1979. He received the M.E. and PhD degrees in electrical engineering from the University of Oviedo, in 2003 and 2007, respectively. He is currently an Associated Professor in the Electrical Engineering Department, University of Oviedo.

From 2004 to 2008, he was awarded and fellowship of the Personnel Research Training Program funded by Regional Ministry of Education and Science of the Principality of Asturias. He was a visitor scholar at the Wisconsin Electric Machines and Power Electronics Consortium, University of Wisconsin, Madison, in 2007. He was a visitor professor at the University of Sheffield (UK), Electrical Machines and Drives Group, in 2016. He was the recipient of nine IEEE Industry Applications Society Conference and IEEE Energy Conversion Congress and Exposition prize paper awards. His research interests include sensorless control of induction motors, permanent magnet synchronous motors and digital signal processing.



**Diego F. Laborda** received the B.S. degree in industrial electronic engineering in 2016 and the M.S. degree in electric energy conversion and power electronics engineering in 2018, from the University of Oviedo, Gijón, Spain, where he is currently working toward the Ph.D. degree in electrical engineering. He has been a Researcher with the Department of Electrical, Electronic, Computers and Systems Engineering, University of Oviedo, since 2018. His research interests include electric machines and power electronics for measurement systems, and digital signal



**Fernando Briz** received the M.S. and Ph.D. degrees from the University of Oviedo, Gijón, Spain, in 1990 and 1996, respectively. He is currently a Full Professor with the Department of Electrical, Computer and Systems Engineering, University of Oviedo. His research interests include electronic power converters and ac drives, power systems, machine monitoring and diagnostics, and digital signal processing. He is a member of the Executive Board of ECCE. He was a recipient of the IEEE Transactions on Industry Applications Award and the nine IEEE Industry Applications Society Conference and IEEE Energy Conversion Congress and Exposition Prize Paper Awards. He is the Chair of the Industrial Power Conversion System Department (IPCS) of the IAS. He is the Past Chair of the Industrial Drives Committee of IPCS. He has served for scientific committees and as the Vice Chair or the Technical Program Chair for several conferences, including ECCE, IEMDC, ICEM, ICEMS, and SLED. He is the Deputy Editor-in-Chief and a member of the Steering Committee of IEEE Journal of Emerging and Selected Topics in Power Electronics. He is an Associate Editor of IEEE Transactions on Industry Applications.



**Daniel Fernandez** received the M.S. degree in power electronic engineering and the Ph.D. degree in electrical and electronic engineering from the University of Oviedo, Gijón, Spain, in 2013 and 2017, respectively. From July to December 2013, he was an Intern with the Nissan Advanced Technology Center, Japan. From August to November 2015, he was a Visiting Student with the University of Sheffield, and from May to July 2019, he was a visiting Professor with the University of Padova.

He is currently an Assistant Professor with the University of Oviedo. His research interests include design, control, and diagnostics of electric machines and drives. Mr. Fernandez was the recipient of a Fellowship of the Personnel Research Training Program funded by the Regional Ministry of Education and Science of the Principality of Asturias in 2013. He was also the recipient of the University of Oviedo Outstanding Ph.D. Thesis Award in 2018.